Microwave spectroscopy of interacting Andreev spins

Wesdorp, J. J.; Vaartjes, A.; Grünhaupt, L.; Roelofs, S.; Splitthoff, L. J.; Pita-Vidal, M.; Bargerbos, A.; Kouwenhoven, L. P.; Andersen, C. K.; More Authors

DOI
10.1103/PhysRevB.109.045302

Publication date
2024

Document Version
Final published version

Published in
Physical Review B

Editors' Suggestion

Microwave spectroscopy of interacting Andreev spins

J. J. Wesdorp,[1,*] F. J. Matute-Cañadas,[4] A. Vaartjes,[1] L. Grünhaupt,[1] T. Laeven,[2] S. Roelofs,[1] L. J. Splitthoff,[1] M. Pita-Vidal,[1] A. Bargerbos,[1] D. J. van Woerkom,[2] P. Krogstrup,[3] L. P. Kouwenhoven,[1] C. K. Andersen,[1] A. Levy Yeyati,[4] B. van Heck,[2,5,6] and G. de Lange[2,†]

[1]*QuTech and Kavli Institute of Nanoscience, Delft University of Technology, 2628 CJ Delft, The Netherlands*
[2]*Microsoft Quantum Lab Delft, 2628 CJ Delft, The Netherlands*
[3]*NNF Quantum Computing Programme, Niels Bohr Institute, University of Copenhagen, 2100 Copenhagen, Denmark*
[4]*Departamento de Física Teórica de la Materia Condensada, Condensed Matter Physics Center (IFIMAC) and Instituto Nicolás Cabrera, Universidad Autónoma de Madrid, 28049 Madrid, Spain*
[5]*Leiden Institute of Physics, Universiteit Leiden, Niels Bohrweg 2, 2333 CA Leiden, The Netherlands*
[6]*Dipartimento di Fisica, Sapienza Università di Roma, P.le Aldo Moro 2, 00185 Roma, Italy*

(Received 12 December 2022; revised 15 November 2023; accepted 16 November 2023; published 3 January 2024)

Andreev bound states are fermionic states localized in weak links between superconductors which can be occupied with spinful quasiparticles. Microwave experiments using superconducting circuits with InAs/Al nanowire Josephson junctions have recently enabled probing and coherent manipulation of Andreev states but have remained limited to zero or small magnetic fields. Here, we use a flux-tunable superconducting circuit compatible in magnetic fields up to 1 T to perform spectroscopy of spin-polarized Andreev states up to ∼250 mT, beyond which the spectrum becomes gapless. We identify singlet and triplet states of two quasiparticles occupying different Andreev states through their dispersion in magnetic field. These states are split by exchange interaction and couple via spin-orbit coupling, analogously to two-electron states in quantum dots. We also show that the magnetic field allows to drive a direct spin-flip transition of a single quasiparticle trapped in the junction. Finally, we measure a gate- and field-dependent anomalous phase shift of the Andreev spectrum, of magnitude up to $\sim 0.7\pi$. Our observations demonstrate alternative ways to manipulate Andreev states in a magnetic field and reveal spin-polarized triplet states that carry supercurrent.

DOI: 10.1103/PhysRevB.109.045302

I. INTRODUCTION

Experimental results in recent years have advanced our understanding of the Josephson effect in terms of Andreev bound states (ABS) [1–3]. When two superconductors (S) are separated by a normal (N) material, the transport of Cooper pairs between them is mediated by Andreev reflections at the N-S interfaces. The consequent formation of current-carrying, discrete Andreev states in S-N-S junctions can be observed with microwave spectroscopy [4–15].

In *s*-wave superconductors, which preserve time-reversal symmetry, Cooper pairs are formed with opposite spins in singlet states with zero total spin. On the other hand, in semiconductors with strong spin-orbit coupling that are proximitized by an *s*-wave superconductor [16,17], a parallel magnetic field can induce a triplet *p*-wave component in the superconducting pairing due to the competition of the spin-orbit interaction and the Zeeman effect [18–21]. Such triplet pairing is of fundamental interest, in part because it is a key ingredient to creating topological superconducting phases with Majorana zero modes [22–24].

The consequences of triplet pairing on the Josephson effect have been widely investigated theoretically and include the occurrence of the anomalous Josephson effect and of spin-polarized supercurrents [25–29]. The experimental detection has, however, proven more challenging. Early signatures of triplet supercurrent have been reported in Josephson junctions with magnetic materials [30–33] and more recently in experiments making use of materials with spin-orbit coupling to induce spin mixing [34–37]. In hybrid semiconductor-superconductor systems, a precursor of triplet pairing stems from the observation of the anomalous Josephson effect in InAs/Al nanowires [38,39] and in two-dimensional electron gases (2DEGs) [40]. Additionally, there are indications of triplet pairing from microwave susceptibility measurements of resonators made out of InAs/Al 2DEGs [41] and from spin-polarized crossed Andreev reflection in InSb/Al nanowires [42]. Evidence of spin-polarized triplet pairs based on microwave absorption and their associated supercurrent has, however, been elusive.

Embedding nanowire Josephson junctions in microwave superconducting circuits allows for probing of individual Andreev states with a remarkable energy resolution of ∼100 MHz (i.e., ∼0.4 μeV) [8–15] and with potential spin sensitivity [9–13]. Thus, such circuits provide an excellent platform to study the (spin) properties of Andreev bound states. In fact, microwave spectroscopy has already revealed

*j.j.wesdorp@tudelft.nl
†gijs.delange@microsoft.com

that spin-orbit coupling [9,10] and electron-electron interactions [14,15] are crucial ingredients that determine the many-body Andreev spectrum of hybrid nanowire Josephson junctions. However, so far, such experiments using superconducting circuits have been limited to zero or small magnetic fields.

In this work, we demonstrate measurements of the Andreev spectra of an InAs/Al nanowire Josephson junction embedded in a superconducting circuit with magnetic fields up to ∼250 mT. The magnetic field dependence of the microwave absorption spectrum shows clear signatures of excited Andreev levels in a triplet state. The spectrum can be well understood based on a minimal model which includes spin-orbit coupling, the Zeeman effect, and ferromagnetic exchange interaction between Andreev bound states, originating from electron-electron interactions in the junction. A particularly interesting feature of the data is the presence of a singlet-triplet avoided crossing. Due to quasiparticle poisoning [43], the microwave absorption spectra also reveal transitions between odd-parity states, which were recently used to realize Andreev spin qubits [11]. Here, we detect the direct driving of the spin-flip transition of an Andreev bound state, activated by the magnetic field. Finally, at high fields we observe a gate-tunable anomalous Josephson effect and resolve the individual contributions of Andreev bound states to the anomalous phase shift. In the next section, we kick off the presentation of our results by discussing the experimental setup and the ingredients that made these measurements possible.

II. FIELD-COMPATIBLE DESIGN AND OPERATION

Previous microwave experiments probing Andreev states with superconducting circuits have traditionally used thick (150-nm) coplanar waveguides [5,9,12,15] or coplanar stripline resonators [8,10,11,14]. Here, we use thin-film (20-nm) lumped-element resonators due to their proven resilience to parallel fields shown earlier in fluxonium devices [44]. Additionally, the second harmonic of the resonator is expected to be at higher frequencies (28.5 GHz, see Supplemental Material [45]) relative to the lowest mode compared to a coplanar geometry of equal fundamental frequency. This helps with spectroscopic measurements at frequencies up to the superconducting gap $\Delta \approx 44$ GHz.

We fabricate multiple resonators on a chip, one of which is shown in Fig. 1(a). The resonator is coupled to a common feed line that is used for microwave readout. The lumped-element resonator, with resonance frequency $f_0 = 4.823$ GHz, consists of a capacitor ($C_r \approx 47$ fF) that is connected to the ground plane via an inductor ($L_r \approx 22$ nH). The inductance is dominated by the kinetic inductance of the thin-film NbTiN [46]. The inductor has a width of 300 nm, such that the required perpendicular field for vortex generation corresponding to one magnetic flux quantum through 300^2 nm^2 is >20 mT in locations where the current is strongest. This is well above perpendicular fields expected due to misalignment when using a vector magnet. We patterned vortex traps with a diameter of 80 nm within an 8-μm radius in the capacitor and surrounding ground planes with a 200-nm gap from structure edges to prevent flux jumps due to moving vortices [47,48]. The inductor

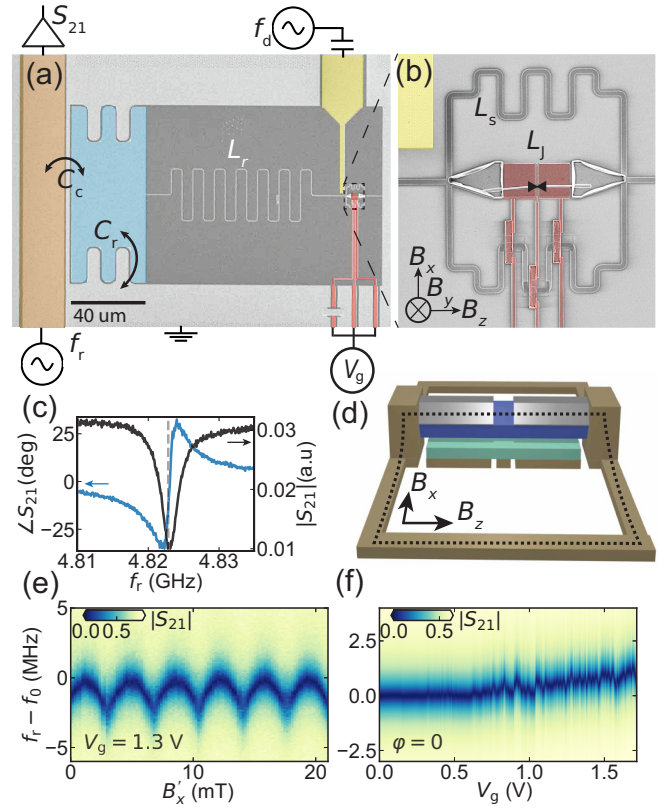

FIG. 1. Field-compatible circuit design and operation principle. (a) Device image and circuit schematic. A lumped element resonator is capacitively coupled (C_c) to a transmission line (orange). The resonator consists of a capacitor (blue) with capacitance C_r to the ground (light gray), and inductor (L_r, white) connected to the ground via a gradiometric RF-SQUID that modulates the total inductance. (b) The SQUID consists of two loops of inductance L_s that shunt a nanowire Josephson junction with gate-tunable Josephson inductance L_J. A drive line (yellow) is used for spectroscopy at frequency f_d. The gradiometric design reduces sensitivity to perpendicular field B_y and the shunt inductance determines the coupling strength to Andreev bound states in the junction. The magnetic field coordinate system aligned to the nanowire and used throughout the text is indicated [45]. (c) Amplitude and phase response of the resonator when the junction is pinched off. (d) Three-dimensional sketch of the SQUID loop. An InAs nanowire (blue) with Al shell (silver) and a 144-nm junction [13] is suspended on gate dielectric (teal) above bottom gates (gold). By applying an in-plane field B_x, we can thread a flux through a vertically defined loop (dashed dots). (e) SQUID oscillations when applying B_x'. (f) Gate dependence of the junction without applying flux. f_0 increases as the critical current (inductance) of the junction increases (decreases).

is connected to the ground via a gradiometric radio-frequency superconducting quantum interference device (RF-SQUID) [Fig. 1(b)] [44], which consists of a nanowire Josephson junction shunted on two sides by an inductance ($L_s \approx 0.7$ nH), forming two nearly equal sized loops. We define a Josephson junction by selectively etching away a 144-nm section in a ∼6-nm-thick aluminum shell that covers two facets of a hexagonal InAs nanowire of ∼80-nm diameter [49]. The nanowire is placed on bottom gates defined in the NbTiN layer, which are covered with a 28-nm Si_3N_4 dielectric before

nanowire placement. To each resonator, we add capacitive coupling to an additional transmission line to drive transitions in the junction and perform spectroscopy.

The specific gradiometric loop design [Figs. 1(b) and 1(d)] was optimized to allow for flux-biased measurements in high magnetic field. The phase difference over the junction $\varphi = 2\pi\Phi/\Phi_0$ can be tuned by applying a flux Φ through the SQUID, where $\Phi_0 = h/2e$ is the magnetic flux quantum. In a gradiometric geometry, the two loops create opposite circulating currents through the nanowire Josephson junction under applied flux by out-of-plane field B_y (see Supplemental Material [45]). The effective loop area is therefore proportional to the area difference between the loops, which here is determined by the inaccuracy of the nanowire placement with respect to the center axis of the two loops ($\sim$300 nm). The resulting effective loop area ($\sim 0.77\,\mu\text{m}^2$, $\Phi_0 \sim 2.6$ mT) is much smaller than the individual patterned loop areas ($\sim 50\,\mu\text{m}^2$) and those used in previous works ($>1000\,\mu\text{m}^2$) that did not measure Andreev spectra in substantial magnetic fields [8–11]. A small effective loop is desired to render the SQUID insensitive to flux from out-of-plane field (B_y), reducing flux noise in the presence of strong external fields. The gradiometric design also allows for picking a shunt inductance L_s—which determines the coupling strength to the Josephson junction—nearly independent of the loop size, which makes for easier design and fabrication.

Additionally, our device design exploits the nanowire placement for optimal flux tuning. That is, by placing the nanowire on top of the bottom gates, we lift the nanowire and thus elevate part of the loop vertically in the z-y plane [Fig. 1(d)]. This allows flux biasing the SQUID with an in-plane field B_x parallel to the rest of the superconducting circuit. Since the magnetic field B_x induces currents flowing in the same direction through the nanowire Josephson junction, the effective flux is proportional to twice the out-of-plane loop area ($A = 0.28\,\mu\text{m}^2$, $\Phi_0 \sim 3.65$ mT). This is shown in the measured SQUID oscillations on the device over a range of 20 mT [Fig. 1(e)]. Due to the thin-film NbTiN, the area of superconducting film that is exposed to parallel field B_x is much smaller compared to the area exposed to perpendicular field B_y. This is essential for flux biasing without flux jumps (see Supplemental Material [45] for a comparison between tuning with B_x and B_y), because vortex nucleation and circulating currents are proportional to the total area of superconducting film exposed to magnetic field [50,51].

Throughout this work we define $\vec{B}$ as the magnetic field aligned to the chip plane and with z along the nanowire axis [Fig. 1(d)] and $\vec{B}'$ as the magnetic field direction output by each of the coils of the used vector magnet (see Supplemental Material for the alignment procedure [45]). We operationally define Φ as $\Phi = B'_x/3.65\,\text{mT} + c$, where c is an offset added to compensate for fluxoids trapped in the outer loop, flux due to the B'_x component of applied B_z, and a small residual ($\sim 0.05\Phi_0$, see Supplemental Material [45]).

We operate the devices by sending a near-resonant probe tone at frequency f_r through the feed line and monitoring the transmitted complex scattering parameter S_{21} using a vector network analyzer. Out of the four resonators we focus on the only one in which the junction showed considerable gate response ($f_0 = 4.823$ GHz). At $f_r = f_0$ there is a dip in the magnitude $|S_{21}|$ and a $\sim 60^\circ$ shift in the phase $\angle S_{21}$ [Fig. 1(c)]. The Josephson junction then acts as a gate- and flux-tunable inductor L_J [Fig. 1(b)] that changes f_0 via

$$f_0 = \frac{1}{2\pi\sqrt{(L_r + L_{\text{squid}})C}},$$

where $L_{\text{squid}}^{-1} = L_J^{-1} + 2L_s^{-1}$. Thus, by monitoring changes in f_0 we get access to L_J, which is related to the Andreev bound state energies and their occupation [52–54]. As we increase the gate voltage V_g on the bottom gates, we observe a trend that more current-carrying channels start to conduct in the junction, which decreases L_J and increases f_0 [Fig. 1(f)]. The smaller modulations on top of the general trend can be attributed to mesoscopic fluctuations of the transparency of individual Andreev states [55,56]. As shown later, we use this to tune the Andreev energies over a large range within small mV gate ranges. From the change in inductance at $\varphi = 0$ between the junction being in an open configuration ($V_g = 1.68$ V) and pinched off ($V_g = 0$ V, $L_J = \infty$), we estimate $L_J = 38$ nH at $V_g = 1.68$ V, resulting in an estimate for the maximal critical current $I_c \approx \varphi_0/L_J = 8.5$ nA. In general, the Andreev states induce a state-dependent frequency shift [12] which generates changes in $\angle S_{21}$ monitored at f_r. This allows us to perform spectroscopy by sweeping a drive tone f_d via the drive line, which results in changes in $\angle S_{21}$ when f_d is equal to an energy difference between Andreev levels of the same parity.

III. ANDREEV BOUND STATE SPECTRUM

In a nanowire Josephson junction, Andreev states arise due to constructive interference after consecutive Andreev reflections from the hybrid superconducting leads [1,2] [Fig. 2(a)]. The energy of an Andreev state depends on an energy-dependent phase gained while Andreev reflection occurs, as well as a phase gained while traversing the junction. In the presence of time-reversal symmetry, which holds at $\varphi = 0$ or $\varphi = \pi$ when the magnetic field is zero, the Andreev energies are twofold degenerate because of Kramers' theorem. The number of Kramers doublets (manifolds) present below the gap depends on the number of the occupied subbands in the leads, and on the length of the junction. In what follows, we restrict our attention to the two lowest manifolds of Andreev levels, labeled a and b [57].

Recent works have highlighted the importance of both spin-orbit interaction [9,10,13,58] and electron-electron interaction [14,15] to understand the Andreev spectrum of nanowire Josephson junctions. While Andreev bound states are spin degenerate at all phases in the absence of spin-orbit interaction, the latter may lift the degeneracy away from $\varphi = 0$ and $\varphi = \pi$. This occurs in junctions of finite length such that a phase shift accumulated due to a spin-dependent Fermi velocity becomes relevant [25,28,58–63], see Fig. 2(b). The typical phase dispersion of the resulting spin-split manifolds is illustrated in Fig. 2(c). As inferred in Refs. [15,64], electron-electron interaction manifests itself via a ferromagnetic exchange interaction $-J\vec{S}^2$ between two quasiparticles in a state of total spin $\vec{S}$, each occupying a different manifold.

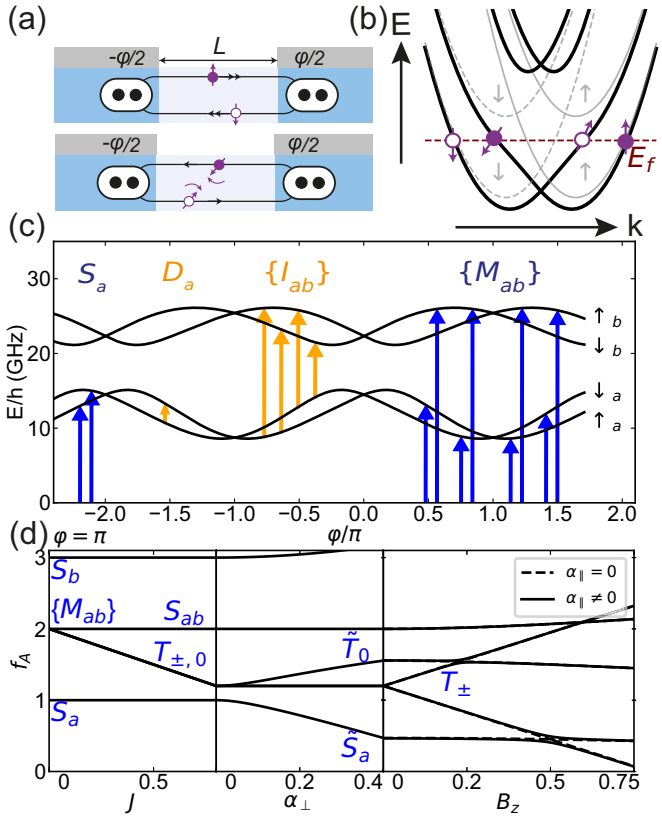

FIG. 2. Hybrid nanowire Josephson junction hosting spin-split Andreev bound states at zero field. (a) Schematic of two Andreev reflection processes in the nanowire junction. Spin-orbit-induced subband hybridization rotates the spins of the bottom Andreev states and lowers the Fermi velocity (v_F). Note that the time-reversed processes are also possible (not shown), and that the Andreev states are generally superpositions of these four Andreev reflection processes. (b) Electron band structure indicating hybridized subbands due to spin-orbit interaction. The anticrossings lead to a rotated spin of the inner Andreev mode and a spin-dependent v_F. (c) Phase dependence of two low-lying spinful Andreev manifolds (a, b) in the noninteracting picture [9]. Arrows denote possible parity-conserving microwave transitions. Pairs of blue arrows indicate even-parity transitions starting from the ground state. Yellow arrows indicate transitions starting from one of the two lowest levels occupied with a quasiparticle. (d) Evolution of even-parity transitions at phase difference $\varphi = \pi$ using Eq. (1), illustrating the effect of exchange interaction J, spin-orbit interaction, and Zeeman energy using $\alpha_{||} < J < \Delta$, which resembles the experiment. J splits the four mixed states $\{M_{ab}\}$ into a singlet S_{ab} and three triplet transitions $\{T\} = \{T_0, T_+, T_-\}$. Spin-orbit interaction hybridizes T_0 and S_a, moving the now hybridized $\tilde{T}_0$ up and $\tilde{S}_a$ down in energy. Finally, a magnetic field splits $T_\pm$.

We now present a minimal model that captures the combined effect of spin-orbit interaction, exchange energy, and the Zeeman effect of an external magnetic field on the two manifolds, restricting our attention to the case $\varphi = \pi$. To do so it is convenient to consider the Andreev states $\{|\downarrow_a\rangle, |\uparrow_a\rangle, |\downarrow_b\rangle, |\uparrow_b\rangle\}$ belonging to the a or b manifold and with spin up or down with respect to the z axis, running parallel to the nanowire. Denoting with $\gamma^\dagger_{i\sigma}$ the operator which creates a quasiparticle with spin σ in the $i = a, b$ manifold, the model Hamiltonian is

$$H = \sum_{i,\sigma} (E_i + \sigma g_i^* B_z)\gamma^\dagger_{i\sigma}\gamma_{i\sigma} - J/2\vec{S}^2 + \sum_\sigma i\bar{\sigma}\alpha_\perp \gamma^\dagger_{a\sigma}\gamma_{b\sigma} + i\alpha_\parallel \gamma^\dagger_{a\bar{\sigma}}\gamma_{b\sigma} + \text{H.c.}. \quad (1)$$

Here, E_i is the energy of the Andreev manifold in the absence of spin-orbit interaction; B_z is the parallel magnetic field and g_i^* is an effective g factor which can depend on the manifold; $\vec{S} = \frac{1}{2}\sum_{i,\sigma,\sigma'} \gamma^\dagger_{i\sigma}(\vec{\sigma})_{\sigma,\sigma'}\gamma_{i\sigma'}$ is the total spin, where $\vec{\sigma}$ is the vector of Pauli matrices; and finally, $i\alpha_{||}$ and $i\alpha_\perp$ are the matrix elements of the spin-orbit interaction described with a two-dimensional (2D) Rashba model, respectively in the direction parallel and perpendicular to the nanowire. More details about each term are given in the Supplemental Material [45].

Within this minimal model, it is straightforward to find the single-particle and two-particle energy levels, which determine the transitions measured in spectroscopy. In particular, the simultaneous occupation of the junction by two quasiparticles results in six possible states. These are two singlet same-manifold states $|S_a\rangle = |\uparrow_a\downarrow_a\rangle$ and $|S_b\rangle = |\uparrow_b\downarrow_b\rangle$ as well as four states corresponding to a mixed occupation of the two manifolds. For the latter, it is natural to pick the basis of simultaneous eigenstates of $\vec{S}^2$ and S_z. These are the singlet $|S_{ab}\rangle = (|\uparrow_a\downarrow_b\rangle - |\downarrow_a\uparrow_b\rangle)/\sqrt{2}$ and the triplet states $|T_0\rangle = (|\uparrow_a\downarrow_b\rangle + |\downarrow_a\uparrow_b\rangle)/\sqrt{2}$, $|T_+\rangle = |\uparrow_a\uparrow_b\rangle$, and $|T_-\rangle = |\downarrow_a\downarrow_b\rangle$. Note that without exchange interaction, a more natural basis of mixed states would be $\{|T_-\rangle, |\uparrow_a\downarrow_b\rangle, |\downarrow_a\uparrow_b\rangle, |T_+\rangle\}$. Also, note that spin-orbit interaction breaks spin-rotation symmetry by hybridizing spin and spatial degrees of freedom. Therefore, in its presence, spin is in general not a good quantum number, and the singlet and triplet states hybridize. Nevertheless, for many parameter regimes the eigenstates of Eq. (1) are well approximated by the singlet or triplet states, with expectation values of the spin close to zero and one. With this in mind, in the rest of the manuscript we will for simplicity keep referring to singlet, doublet, and triplet states, except in cases where spin-orbit effects change this simple picture appreciably.

In microwave spectroscopy, we only have access to transitions between many-body states of the same fermion parity. In Fig. 2(c) we label the possible transitions in both even- and odd-parity sectors. In the even-parity sector, we only consider transition from the ground state of the junction $|0\rangle$, with no quasiparticle excitations. There are therefore six possible transitions (pairs of blue arrows, the transition to $|S_b\rangle$ is not shown), which we will denote by their final state. The lowest energy transition is the singlet pair transition S_a from $|0\rangle$ to $|\uparrow_a\downarrow_a\rangle$. The four transitions that involve breaking a Cooper pair and splitting over the two different manifolds a and b will be globally denoted as $\{M_{ab}\}$ [blue arrows on the right side of Fig. 2(c)]. Note that these four transitions are degenerate in the absence of spin-orbit interaction and exchange interaction.

In the odd-parity sector, we denote the lowest doublet intramanifold transitions as $D_a : |\uparrow_a\rangle \leftrightarrow |\downarrow_a\rangle$. This is a direct spin-flip of a quasiparticle occupying the lowest Andreev manifold [left yellow arrow in Fig. 2(c)]. Furthermore, we denote the set of four inter-manifold transitions of a single quasiparticle from $\{|\uparrow_a\rangle, |\downarrow_a\rangle\}$ to $\{|\uparrow_b\rangle, |\downarrow_b\rangle\}$ as $\{I_{ab}\}$ [set of yellow arrows in Fig. 2(c)]. In the data presented in

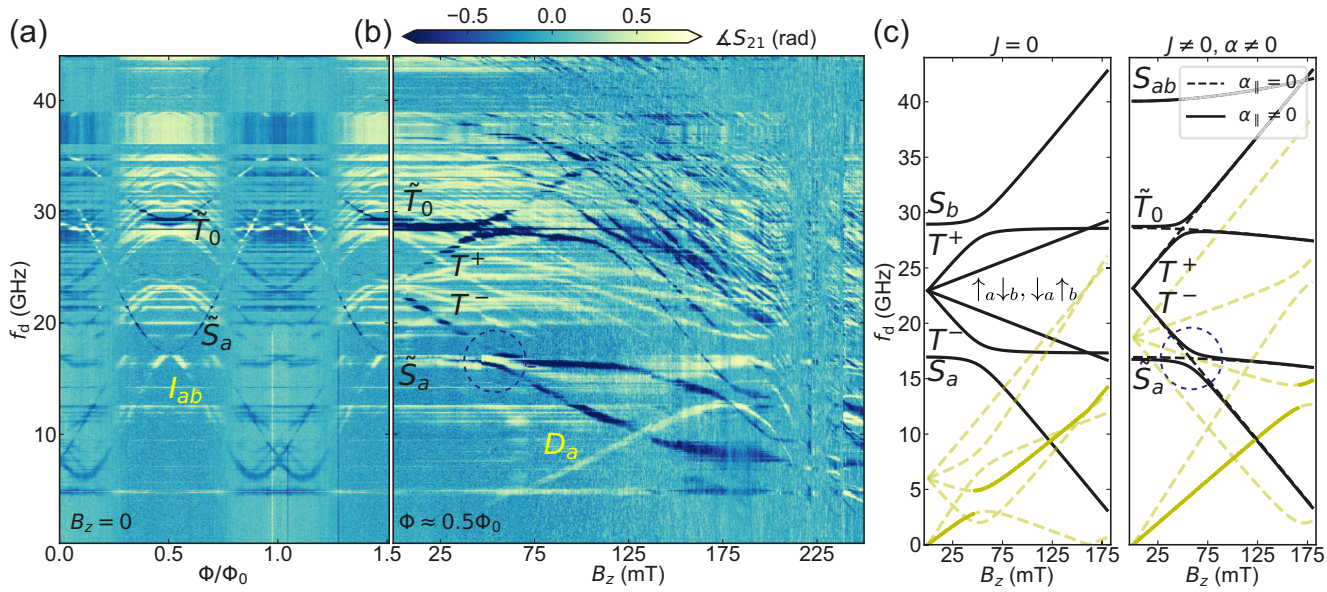

FIG. 3. Spectroscopy of singlet, doublet, and triplet Andreev states versus flux and magnetic field. (a) Measured spectrum at zero field versus external flux Φ at $V_g = 625\,\mathrm{mV}$. (b) Evolution of Andreev transition spectrum in an aligned parallel magnetic field starting from the right side of (a) ($\Phi \approx \Phi_0/2$). At low fields, the transitions disperse linearly with B_z and we can distinguish transitions to singlet, doublet, and triplet Andreev states as indicated. At higher fields, a plethora of Andreev transitions move downwards until the low-energy spectrum becomes very crowded and visibility low. Note that $\Phi \approx \Phi_0/2$ holds only for $B_z < 160\,\mathrm{mT}$, after which Φ changes nonlinearly with B_z. (c) Fit to minimal theoretical model at $\varphi = \pi$ including α and exchange interaction J (see Supplemental Material [45]). Black lines indicate even-parity transitions with types indicated. Also indicated are the interband I_{ab} (yellow dashed lines), the lowest doublet spin-flip transition D_a (yellow full line), and D_b (yellow dashed line starting from the same point), which is not visible in the data (see discussion in Sec. V of the main text). Left plot indicates a best fit when assuming $J = 0$ and the top even transition excites a second subband S_b. When $J = 0$, two more transitions (S_{ab}, T_0) should appear that are not in the data and I_{ab} should appear at low frequency. Right plot is best fit with $J = 17\,\mathrm{GHz}$, $\alpha_\perp = 4.8\,\mathrm{GHz}$. Here, the even-parity transitions and I_{ab} match the data (see Supplemental Material for lines on top of the data [45]). Note that $\alpha \neq 0$ hybridizes the singlet S_a and triplet T_0, denoted as $\tilde{S}_a$ and $\tilde{T}_0$, respectively. The avoided crossing between T_- and $\tilde{S}_a$ only occurs in the presence of a spin-orbit component $\alpha_{||}$ along the wire.

Sec. IV, we find signatures of more manifolds present at higher energies, due to additional intermanifold transitions, i.e., $\{I_{ac}\}$, $\{I_{ad}\}$. However, because the even-parity transitions corresponding to those manifolds are at frequencies outside the measurement range at zero magnetic field and only appear at higher fields, we restrict the modeling and data analysis to the lowest two manifolds a, b.

In Fig. 2(d) we sketch the resulting modifications to the two-particle spectrum as predicted by the model of Eq. (1). The exchange interaction lowers the energy of the triplet states and, in doing so, partially lifts the degeneracy between the singlet transition and triplet transitions [Fig. 2(d), left panel]. The role of spin-orbit interaction is different: it breaks the spin-rotation symmetry and lifts the degeneracy of single-particle states away from the time-reversal invariant points $\varphi = 0, \pi$. The combination of spin-orbit interaction and exchange interaction can completely lift the degeneracy of the triplet states even at $\varphi = 0, \pi$ [15]. In the minimal model, this occurs partially, by hybridizing $|T_0\rangle$ and $|S_a\rangle$. We will denote the transitions to the hybridized states $|\tilde{T}_0\rangle$ and $|\tilde{S}_a\rangle$ by $\tilde{T}_0$ and $\tilde{S}_a$, respectively [Fig. 2(d), middle panel]. The remaining degeneracy within the manifold of two-particle states, that of the triplet states $|T_\pm\rangle$, is lifted by the external magnetic field via the Zeeman effect [Fig. 2(d), right panel].

IV. ANDREEV SPECTROSCOPY: SINGLET, DOUBLET, AND TRIPLET TRANSITIONS

With the theory developed, we now continue with the measurement results. We first measure the junction spectrum at zero magnetic field versus applied flux Φ [Fig. 3(a)]. The gate is set to $V_g = 625\,\mathrm{mV}$, where we have a few Andreev transitions present and the spectrum is dominated by the lowest two manifolds (see Supplemental Material for additional gate dependence [45]). Due to the presence of quasiparticle poisoning, the junction fluctuates between the even-parity ground state $|0\rangle$ with no Andreev level occupied and, when a quasiparticle has entered the junction due to a poisoning event, one of the odd-parity doublet states $|\uparrow_a\rangle$, $|\downarrow_a\rangle$. In a related work performed on the same junction, we measured typical poisoning times of $\sim$0.5 ms [13], much smaller than the integration time per point $\sim$100 ms: thus, the measured spectra are an average of those resulting from initial states with and without a quasiparticle. Odd- and even-parity transitions can be distinguished by their opposite sign in the dispersive frequency shift induced on the resonator [12] and characteristic dispersion. For instance, the phase response near $\Phi = \Phi_0/2$ is negative (blue) for even parity and positive (yellow) for odd parity.

We first establish that we detect the same types of transitions as in recent experimental works [9,10,13]. These are the even-parity transition with parabolic dispersion around 16 GHz at $\Phi = \Phi_0/2$, and the transitions starting from the poisoned doublet state, I_{ab}, with the characteristic "spider-like" shape due to the spin-orbit splitting of the Andreev levels in manifolds a and b. Note that the lowest bundle is associated with $\{I_{ab}\}$ and higher bundles likely correspond to transitions from manifold a to higher manifolds $c, d, \ldots$ present in the junction at higher energies. We investigate the splitting of the $\{I_{\rm ac}\}$ transitions due to B_x and B_z in the Supplemental Material [45]. A symmetric splitting due to B_z and asymmetric splitting due to B_x was used in Ref. [9] to infer that the direction of the effective magnetic field generated by spin-orbit interaction was in plane and perpendicular to their full-shell nanowire. Here, we do not observe such a clear differentiation between symmetric and asymmetric splitting. This leads us to suspect that the effective spin-orbit field is not parallel to B_x, which is consistent with recent findings indicating that, in partial-shell wires, the spin-orbit direction depends strongly on the direction of the local electric field in the wire, which in turns depends on the position and number of Al facets and gate geometry [65,66].

Furthermore, we see a second even-parity transition dispersing in a similar way as the first, but at higher frequency, with a minimum around 30 GHz. The identification of the final states in the even transitions visible at zero field is resolved later in this section on the basis of the magnetic field dependence. The horizontal bands visible in Figs. 3(a) and 3(b), mostly at higher frequencies, are attributed to resonances in the drive line and connected circuit, resulting in a frequency-dependent driving strength.

Next, we measure a parallel field dependence of the Andreev spectrum, while keeping the gate fixed [Fig. 3(b)], in order to investigate the spin texture of the excited states. By aligning the magnetic field, we keep the phase drop over the junction fixed at $\varphi \approx \pi$ (see Supplemental Material for the alignment procedure [45]) and polarize the spins with B_z [see Fig. 1(d)]. A rich spectrum emerges, with several notable features in both the even and odd transitions.

We start by describing the even-parity spectrum observed in Fig. 3(b). Based on the phase response at $\Phi \approx \Phi_0/2$ in Fig. 3(a) and known dispersion from earlier works [4,5,7,8,15], we can distinguish even-parity transitions as spectral lines with a negative (blue) response. The even transitions observed at 16 GHz and 31 GHz at $B_z = 0$ remain approximately constant at low fields, as expected from a transition to a final state with a small spin polarization, thus essentially insensitive to the Zeeman effect. We also observe two even-parity transitions that disperse linearly in field in opposite directions starting at approximately 24 GHz. We thus infer that the final states reached by these transitions are sensitive to the Zeeman effect and must therefore have some degree of spin polarization along the field direction. The fact that they originate from nearly the same frequency as the bundle of four odd-parity transitions I_{ac} at $\Phi \approx \Phi_0/2$ [visible in Fig. 3(a) at $\sim$23 GHz] is a coincidence and depends on the specific $V_{\rm g}$ set point. Notably, they also display an avoided crossing with the nondispersing even transitions at $B_z \approx$50 mT, confirming that these transitions are of equal parity.

In order to label the even-parity transitions correctly, we first attempt to fit the main features of the spectrum to our model of Eq. (1) without assuming electron-electron interactions. For this, we assume the even transition at 16 GHz in Figs. 3(a) and 3(b) is S_a, while the one at 31 GHz is due to a second Andreev manifold, i.e., the pair transition S_b. We then perform a best fit to the extracted transition frequencies at $B_z = 0$, while imposing a constraint that $J = 0$. While such a fit is possible, this choice of parameters also predicts the presence of two additional spectral lines corresponding to the mixed final states without exchange interaction $\sim |\uparrow_a\downarrow_b\rangle, |\downarrow_a\uparrow_b\rangle$. These even-parity states disperse with the difference of the effective g factors of the two manifolds and should thus appear as two additional lines with a negative (blue) phase response, which are not observed in the field-dependent data. We have investigated, using a standard noninteracting tight-binding model for the nanowire Josephson junction, whether the absence of these transitions could be explained on the basis of a selection rule, i.e., vanishing matrix elements [45]. We have indeed found cases where transitions to $|\uparrow_a\downarrow_b\rangle$ and $|\downarrow_a\uparrow_b\rangle$ have vanishingly small matrix elements at $\varphi = \pi$. However, even in these cases, the noninteracting model predicts them to be typically more visible than T_+ and T_- at phase differences away from $\varphi = \pi$. The latter fact can be understood on the basis that, unlike $|T_+\rangle$ and $|T_-\rangle$, the final states $|\uparrow_a\downarrow_b\rangle$ and $|\downarrow_a\uparrow_b\rangle$ do not require a spin-flip and thus should be more easily observable at small magnetic fields. Overall, this picture is inconsistent with additional measurements of the phase dependence of these states at finite magnetic field (see Supplemental Material [45]), where we did not observe the additional transitions.

Having thus disfavored a scenario based on the absence of interactions between Andreev states, we proceed by analyzing the consequence of setting $J \neq 0$ in Eq. (1). Only in the presence of both a finite spin-orbit interaction $\alpha_\perp, \alpha_{||} \neq 0$ and $J \neq 0$ can we reproduce the spectrum produced by the lowest two manifolds a, b for small magnetic fields, as seen in the data [Fig. 3(c), right panel]. From the fit of the data positions at zero field, we find $J = 17$ GHz and $\alpha_\perp = 4.2$ GHz (see Supplemental Material for lines on top of the data [45]). The extracted exchange is comparable to estimated values of the effective charging energy of the normal region in a similar device ($\sim 0.1\Delta$) [15], and thus singlet-doublet ground state phase transitions are not expected. This is different from the situation reported in Ref. [14] ($\sim\Delta$), or when a quantum dot is gate-defined in the junction, such as in Ref. [67], where the interaction is estimated to be $\sim 10\Delta$. With these parameters, the two even transitions that do not disperse in field in Fig. 3 are identified with the hybridized states $\tilde{S}_a$ and $\tilde{T}_0$, motivating the ordering of transitions displayed in Fig. 2(d). Note that the fit simultaneously takes into account and matches the position of the odd-parity intermanifold transitions I_{ab} (yellow dashed lines) at zero field, visible in Fig. 3(a) but only occasionally and feebly in Fig. 3(b). I_{ab} is more visible at other flux values shown in the phase dependence at finite B_z in the Supplemental Material [45]. The reason why the I_{ac} transitions starting at $\sim$23 GHz in Fig. 3(b) are more visible at $\Phi_0/2$ compared to I_{ab} is presently unclear.

The effective g factors of the Andreev manifolds are not varied in the fit, but fixed to values extracted separately, as

discussed in the next section. From the fit, together with the wire diameter, we can estimate a lower bound on the Rashba spin-orbit strength α_R of $\alpha_R \geqslant 2$ meVnm (see Supplemental Material [45]). This is on the lower side of typical values of 5−40 meVnm found in literature for InAs nanowires [7,9,68,69]. Finally, the avoided crossings between T_- and $\tilde{S}_a$, circled in Fig. 3, and between T_+ and $\tilde{T}_0$ are only reproduced by the model if we include a finite parallel spin-orbit component $\alpha_\parallel$, set to 1 GHz for visibility. The extracted size of the T_-, $\tilde{S}_a$ crossing from the data, approximated by half the frequency difference of the transitions in the center of the crossing, is ~ 0.5 GHz. Overall, the observation of the triplet transitions T_-, $\tilde{T}_0$, T_+, in finite magnetic field, together with the fact that they have a strong phase dispersion (see Supplemental Material [45]), implies that part of the supercurrent flowing in the junction is carried by spin-polarized triplet pairs. From the slope of the transition T_- versus phase at $B_z = 95$ mT, we can estimate a change in current of approximately 2.3 nA with respect to the supercurrent flowing when the junction is in the ground state (see Supplemental Material [45]). This is a measure of the supercurrent carried by the spin-polarized pair.

At higher fields we observe a strong downward trend of the transition frequencies. We suspect that this is dominated by the orbital effect of the magnetic field in the nanowire [70], since the 6-nm aluminum shell has a much higher critical field exceeding 1 T [49]. In the Supplemental Material, we investigate the presence of a revival of the Andreev spectrum in fields up to 1 T [45], motivated by observations of a plasma mode revival on similar nanowires in a transmon geometry [71,72] and supercurrent revival [70] due to interference effects, but we do not find it. The presence of a revival would open up the path towards detection of signatures in the microwave response of a topological phase transition in the presence of multiple Andreev manifolds [73], manifesting as the fractional Josephson effect [18,74].

V. DIRECTLY DRIVEN ANDREEV SPIN-FLIP

So far we have mostly considered the even-parity part of the spectrum of Fig. 3(b). However, when the junction initially is in one of the doublet states due to quasiparticle poisoning, we can distinguish a linearly upward dispersing transition D_a with a positive (yellow) phase response [Fig. 3(b)] at finite field. We attribute this to a directly driven spin-flip between the spin-up $|\uparrow_a\rangle$ and spin-down $|\downarrow_a\rangle$ levels of the lowest Andreev manifold [Fig. 3(c)].

From the slope of D_a we can extract an effective g factor $g_a^* = 5.3$ of the lowest manifold. The triplet transitions T_+ and T_- should disperse in field with the half-sum of the effective g factors of the two manifolds: $g^* = \pm 1/2(g_a^* + g_b^*) = 7.8$. Thus, we infer that the higher doublet has a higher effective g factor of $g_b^* = 10.3$. These values are used for the fit to the theory model presented in Fig. 3(c) and are consistent with hybridized states, where the g factor should be between $|g_{\mathrm{Al}}| \approx 2$ and $|g_{\mathrm{InAs}}| \approx 15$. On the other hand, $\tilde{T}_0$ and S_{ab} disperse weakly in field. We attribute this to a competition between the exchange and the difference in Zeeman energy of each manifold. By solving the model without spin-orbit interaction, the eigenenergies of $|T_0\rangle$ and $|S_{ab}\rangle$ result in

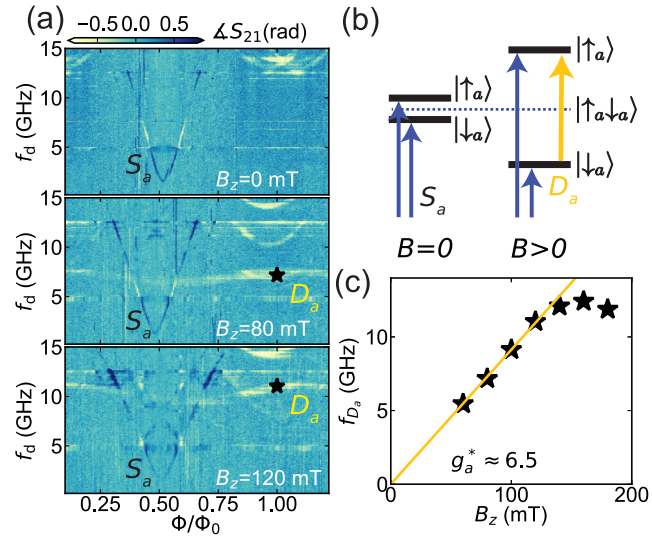

FIG. 4. Phase dependence of the singlet S_a and directly driven spin-flip doublet D_a transition in the lowest Andreev manifold at finite magnetic field. (a) Measured low-energy transition spectra at $V_g = 628$ mV for increasing magnetic fields where the transparency of the lowest Andreev state is at a local maximum. The spin-flip doublet transition is visible at $B_z > 50$ mT. (b) Schematic of the two transitions at zero and finite field. A magnetic field induces a finite matrix element to allow observation of the $D_a : |\uparrow_a\rangle \leftrightarrow |\downarrow_a\rangle$ transition in the spectrum. (c) Extracted doublet transition frequency versus phase at $\Phi = \Phi_0/2$, indicated by stars in (a). The transition evolves linearly versus field until spin-orbit interaction causes the lowest Andreev level to interact with higher levels that come down with B_z, bringing down the transition frequency.

$E_a + E_b - J/2 \pm \sqrt{(J/2)^2 + (\mu_B B_z)^2 (g_a^* - g_b^*)^2}$, which is linear in B_z when $B_z \gg J$ and quadratic in B_z when $B_z \ll J$. Thus, for large fields their dispersion converges to that of the noninteracting states $|\uparrow_a\downarrow_b\rangle$, $|\downarrow_a\uparrow_b\rangle$. A possible cause of the large difference in the g factors of the Andreev manifolds is that the Fermi velocity of the first subband is higher than that of the second subband due to the larger distance from the band bottom. Therefore, the effective spin-orbit strength is higher for the first subband [75], reducing g_a^* more than g_b^*.

We note that we do not observe the intradoublet transition D_b of the higher doublet, which would have a larger slope due to the higher g factor. This can be explained by the fact that the initial state of this transition is too short-lived: any quasiparticle occupying the higher manifold quickly decays into the lowest manifold. A comparison of the measured parity lifetimes $\sim$0.5 ms that we recently reported for this device [13] to measured lifetimes $\sim$4 μs of an excited quasiparticle in the higher manifold in InAs/Al nanowires [10] supports this.

So far, we have exclusively inferred the observation of a direct Andreev spin-flip transition D_a from data at $\Phi \approx \Phi_0/2$. In order to provide additional evidence supporting this observation, we now explore the phase dispersion of D_a [Fig. 4]. To facilitate this, we exploit the gate tunability of the nanowire Josephson junction to move to a nearby gate setting $V_g = 628$ mV, where the lowest manifold has a high transparency and thus D_a is energetically separated from the rest of the spectrum (see Supplemental Material for the gate dependence

at $B_z = 0\,\mathrm{T}$ [45]). In Fig. 4(a) we show the evolution of the phase dispersion when increasing B_z. At $B_z = 0$, we only see the singlet transition S_a. When we increase B_z, we observe both S_a and the odd-parity spin-flip doublet D_a, as indicated in the diagram of Fig. 4(b). As the dispersive shift in the presence of resonator crossings in general can switch signs [12], which would change their color in Fig. 3, we have confirmed the odd-parity nature by performing parity-selective spectroscopy [13] at $B_z = 100\,\mathrm{mT}$ in the Supplemental Material [45]. As expected, the phase dispersion of S_a stays constant at small fields since it is spin-singlet or hybridized with T_0, while D_a moves up in frequency linearly [Fig. 4(c)] with $g_a^* \approx 6.5$. Note that g_a^* differs from the previous gate setting (see Supplemental Material [45]).

The lack of D_a at zero field can be explained by two possible causes. At $B_z = 0$, the steady-state population of $|\uparrow_a\rangle$ and $|\downarrow_a\rangle$ could be nearly equal due to the near-degeneracy in energy, reducing signal when driving D_a. Additionally, the matrix element to drive D_a is expected to vanish at zero field [75] (see Supplemental Material [45]), which is why recent works on coherent manipulation of an Andreev spin qubit [11] were forced to utilize Raman transitions to be able to achieve population transfer. Additionally, recent observations of D_a at zero field [12] indeed observed a vanishing of the transition around $\varphi = \pi$. A finite magnetic field in combination with spin-orbit coupling increases the matrix element, thus facilitating direct driving of this transition at $B > 0$ [thicker yellow line in Fig. 4(b)]. The field also favors the occupation of $|\uparrow_a\rangle$, possibly increasing the population difference and therefore the strength of the signal.

Although S_a has a large dispersion, D_a only has a small phase dispersion ($\sim$2 GHz). This is consistent with expectations, since the dispersion is only caused by the effective spin-orbit splitting of the Andreev levels [58]. Finally, note that the minimum of D_a is not aligned with S_a. Using tight-binding simulations of a similar scenario (see Supplemental Material [45]), we found that a possible explanation could be due to a component of the effective spin orbit field B_{SO} parallel to B_z, consistent with the earlier mentioned field dependence of the interband odd-parity transitions. The observation of the spin-flip transition in a magnetic field opens up the path towards directly driven superconducting spin qubits [60,76] and allows tuning the qubit frequency over a wide range of frequency, depending on the field strength.

VI. GATE-DEPENDENT ANOMALOUS JOSEPHSON EFFECT AT FINITE FIELDS

In Fig. 3(b) we have shown the field evolution at fixed phase difference. The entire phase dispersion is also of interest, because of the possible presence of the anomalous Josephson effect (AJE) [25,28,62,77–81]. To investigate its occurrence, we measured finite-field spectra at different gate voltages, several of which are shown in Fig. 5(a) (see Supplemental Material for all data [45]). We track the minima and maxima of this transition, indicated with the white and black stars, respectively. As we increase the gate voltage, the transition starts to shift horizontally to the left, demonstrating the phase shift in the spectrum. Both even- and odd-parity transitions (offset with a nearly π phase) exhibit a shift.

In Fig. 5(d) we show the extracted shift of the maxima for all measured spectra versus gate, resulting in a continuously gate-tunable relative shift up to $\Delta\varphi = 0.72\pi$ at $V_g = 629\,\mathrm{mV}$ with respect to the reference phase at $V_0 = 620.6\,\mathrm{mV}$. For these measurements, the magnetic field is set to $B_z = 220\,\mathrm{mT}$ and we add a perpendicular component $B_x = 45\,\mathrm{mT}$ (equivalent to $\Phi = 12.3\Phi_0$) [Fig. 5(b)]. The perpendicular component is added to reduce flux jumps due to zero-field crossings. Additionally, we expected the AJE to be stronger in the presence of a perpendicular field component [38,62]. The choice of field was limited in the B_x direction by the maximum output of the current source. Beyond $B_z = 220\,\mathrm{mT}$, we lost visibility in the two-tone spectra.

In essence, the AJE occurs because coupling between different Andreev levels pushes their minima away from $\varphi = 0$ [28,62]. The minimum of the ground state energy, which is a sum over all the Andreev energies, then also shifts away from $\varphi = 0$ and the junction will assume a phase difference that minimizes the ground state energy at $\varphi = \varphi_0$, or, if a phase difference is imposed externally in a loop geometry, a finite current will flow at zero external flux through the loop.

For the AJE to occur, breaking of time-reversal symmetry is a necessary but not sufficient condition. Additional spatial or spin-rotation symmetries need to be broken depending on the setup [82–84]. A Zeeman field breaks time-reversal symmetry and spatial symmetries can be broken by spin-orbit interaction in the presence of a nonsymmetric potential [81] or multiple subbands [28]. In our system we are clearly in a regime with multiple occupied subbands [Fig. 3], evident by the many Andreev transitions visible at higher fields. Due to the asymmetry of the gates with respect to the junction (see device images in Ref. [13]), we would not expect a symmetric potential. Thus, we expect to see the AJE. In recent experiments demonstrating the AJE, measurements of the DC supercurrent [38–40,84], or of the ground state Josephson energy [44], were used to probe the anomalous phase shift caused by the summed contributions of all Andreev levels. In Fig. 5(a) we add to this by showing the underlying microscopic origin of the anomalous supercurrent: the phase shifts of Andreev transitions, which imply shifts of the individual Andreev levels, and which we can measure directly in magnetic fields strong enough to produce this effect.

To compare with supercurrent measurements, we also measure the SQUID oscillations in the resonator in the same gate regime [Fig. 5(c)]. The blue data points in Fig. 5(d) correspond to the maxima in the single tone (ST) resonator traces in Fig. 5(c). The frequency shift of the resonator f_0 originates from the dispersive coupling with the junction in the ground state, and so it is a measure of the phase shift of the ground state current-phase relation of the junction. Since the total φ_0 results from contributions of different channels, which may lead to cancellation if these channels have different phase shifts (see Supplemental Material [45] for a larger frequency range than Fig. 5(a) illustrating the different shifts per Andreev state), it is not surprising that the phase shift in f_0 is smaller than the phase shift of the individual lowest Andreev states in Fig. 5(d).

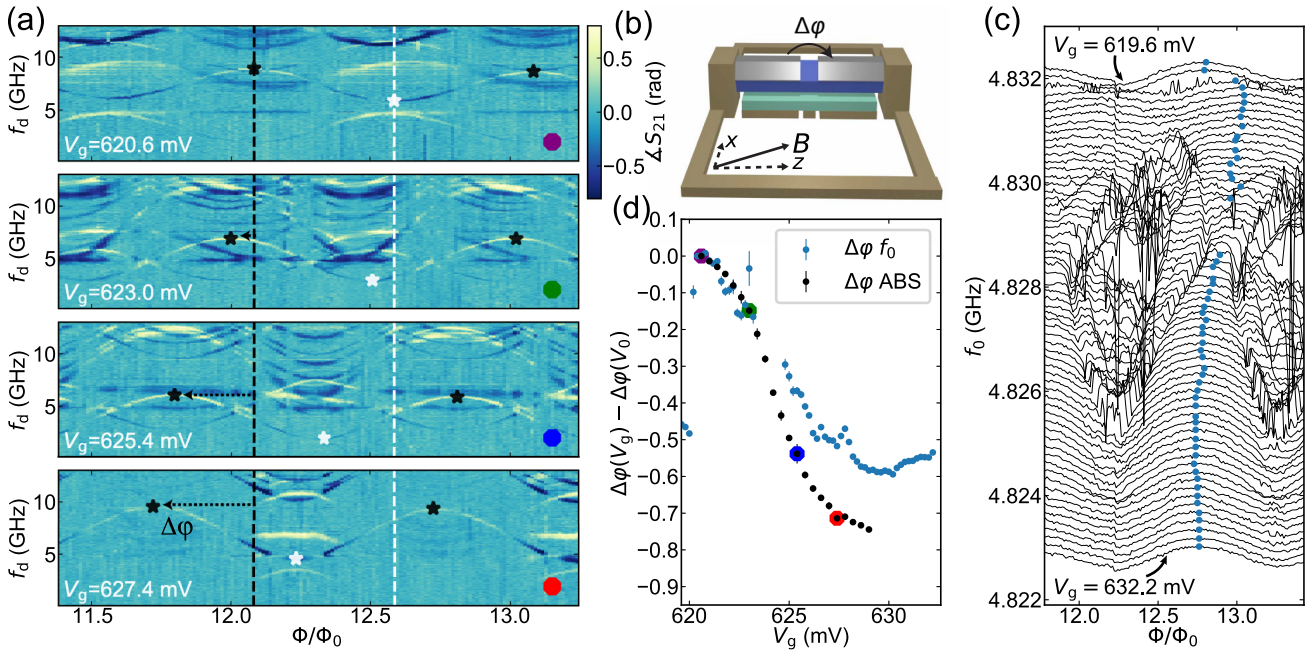

FIG. 5. Gate-dependent anomalous Josephson effect of both individual Andreev transitions and aggregate supercurrent in the presence of finite magnetic field: $B_z = 220\,\mathrm{mT}$ and $B_x = 45\,\mathrm{mT}$. (a) In the two-tone spectra, we follow a transition shifting to the left with increasing gate voltage. We suspect this is an odd-parity transition (see Supplemental Material for the identification and comparison of even- and odd-parity phase shifts [45]). Dashed vertical lines indicate the positions of the maximum (black) and minimum (white) of the reference gate voltage. (b) Diagram of the SQUID loop with B indicating the direction of the field. (c) SQUID oscillations in the resonator frequency in the same field and gate settings as the spectra in (a). They undergo a leftward phase shift with an increasing gate voltage. The blue dots indicate the positions of the maxima for each V_g. The distortion of the lines in the middle region are caused by avoided crossings between Andreev state transition frequencies and the resonator when the transparency of the junction is high. (d) Phase shift extracted from the two-tone excitation spectra [colored markers indicate the corresponding panel in (a)] with respect to a reference gate voltage $V_0 = 620.6\,\mathrm{mV}$. Additionally, the phase shift $\Delta\varphi\ f_0$ extracted from resonator SQUID oscillations (c) are shown.

A gate-induced phase shift can have other explanations different than the AJE, and we now discuss measures we took to rule those out. When sweeping the large vector magnet, flux can be trapped or detrapped on chip or drift over time, which can cause unwanted phase shifts. To rule out flux drift, we measured the three-dimensional (3D) map in the spectra of Fig. 5(a) by sweeping f_d for each V_g before stepping flux. This ensures that the change in phase is caused by V_g. Alternatively, a change in total supercurrent can change the phase drop over the junction when the shunt inductance is large due to a nonlinear relation between Φ and φ. In the Supplemental Material we estimate that we should be in a linear regime for the given L_s and typical I_c [45]. Also, we measured data at lower field strengths and we saw no anomalous shift at $B = 0$ [45]. To exclude a trivial origin of the observed phase shift by a gate-induced change in effective loop size, we have also kept track of the difference between two maxima in the two-tone spectra as an estimate of the total period. We saw no clear correlation with the phase shift. Fluctuations of the period were around $\Delta\Phi = 6\,\mathrm{m}\Phi_0$. This can at most account for a phase shift of $\Delta\varphi = 0.14\pi$, much smaller than what we report here. To further investigate the cause of the gate dependence of the AJE, we performed a series of parallel field sweeps versus gate in the Supplemental Material [45]. Here, by inspecting the D_a transition where it was visible, we extracted g_a^* as a function of V_g, which is correlated with the size of the phase shift. This would indicate the AJE scales with the effective Zeeman energy of the lowest Andreev manifold. We have also performed measurements of the AJE with the field vector reversed, both for the SQUID oscillations and the spectroscopy. Here, we observe a reversal of the phase shift as expected (see Supplemental Material [45]). We thus conclude that the observed phase shift [Fig. 5] is indeed due to the AJE and not due to the alternative causes mentioned above.

VII. CONCLUSIONS

In this work, we have performed microwave spectroscopy of Andreev bound states in a nanowire Josephson junction in a magnetic field, using a field-compatible superconducting resonator. By aligning the magnetic field parallel to the nanowire, we have investigated the field dependence of the many-body spectrum at fixed phase difference over the junction ($\varphi = \pi$), for both even and odd fermion parity. In the even-parity sector, we distinguished singlet- and triplet-like Andreev states, hybridized by spin-orbit interaction and split by exchange interaction. In the odd parity, at finite field, we observed the direct doublet spin-flip transition in the lowest Andreev manifold. At fields larger than $B_z = 170\,\mathrm{mT}$, we

found a strong gate-tunable anomalous Josephson effect in the many-body spectrum, currently of interest due to its envisioned application in spintronics [33]. Our findings confirm that both spin-orbit interaction and electron-electron interactions are important to understand Andreev spectra in InAs/Al Josephson junctions.

The observed hybridization of triplet and singlet Andreev transitions is consistent with predictions that in a finite magnetic field, the induced superconducting pairing in the semiconducting nanowire is a mixture of singlet and triplet components [18,19]. However, our measurements probe states localized at the Josephson junction, which depend on both local and bulk properties, and we cannot exclude that spin-orbit interaction is only active in the junction, but not in the leads. Thus, our measurements should be complemented with methods that can single out the bulk properties of the nanowire [41,85,86].

It remains an open question to explore the dependence of the Andreev spectra on the electron density, in both the proximitized leads and in the junction itself, which is of importance for topological superconductivity. Signatures of topological phase diagrams could be observable in microwave spectroscopy [73,87,88] due to the onset of the fractional Josephson effect, but it seems crucial to extend available theory to understand the effect of interactions and g-factor renormalization. To prevent the closing of the spectral gap due to orbital interference, it would be interesting to perform these measurements in devices with a lower density of states. This could be aided by another choice of material, e.g., InSb, which has a lower effective mass and smaller band offset with Al [89] compared to InAs.

Spectroscopy of Andreev states using superconducting circuitry allow the combination of spectroscopic measurements with high time resolution, allowing, e.g., parity-selective spectroscopy, as we have shown recently at zero field [13]. In the future, when combined with on-chip flux control and parametric amplification readily available in the superconducting circuit community, this combination should allow for fast measurements of the phase periodicity of individual Andreev levels in time scales of GHz to MHz. This type of measurement could provide a more controlled way towards the detection of the fractional Josephson effect, not hindered by the presence of quasiparticle poisoning [18] or Landau-Zener effects [90].

Additionally, the observation of the spin-flip transition as well as a singlet-triplet avoided crossing can provide alternative ways to manipulate Andreev (spin) qubits [5,8,10,11], that exploit an external field. In particular, the direct spin-flip transition activated by the magnetic field makes it possible to circumvent the need to use used Raman techniques [11] involving a second bound state in order to manipulate the spin of an Andreev state [58]. Furthermore, the singlet-triplet avoided crossing is particularly interesting as it opens up the possibility to manipulate Andreev pairs in analogy with singlet-triplet qubits in semiconducting quantum dots [91,92].

Data, processing, and scripts for the presented figures are available online via Ref. [104].

ACKNOWLEDGMENTS

We would like to thank Ruben Grigoryan for the PCB and enclosure design; Guanzhong Wang, Tom Dvir, and Cyril Metzger for useful discussions; and Valla Fatemi for valuable comments on the manuscript. This work is part of the research project "Scalable circuits of Majorana qubits with topological protection" (i39, SCMQ), Project No. 14SCMQ02, which is (partly) financed by the Dutch Research Council (NWO). It has further been supported by the Microsoft Quantum initiative. F.M.C. and A.L.Y. acknowledge funding by FET-Open contract AndQC, by the Spanish AEI through Grant No. PID2020-117671GB-I00, by the "María de Maeztu" Programme for Units of Excellence in R&D (CEX2018-000805-M), and by the Spanish Ministry of Universities (FPU20/01871).

J.J.W., B.v.H., G.d.L., D.v.W., and S.R. contributed to the device design. J.J.W., A.V., L.J.S., and M.P.V. contributed to sample fabrication and inspection. J.J.W. and A.V. contributed to the data acquisition and analysis with input from G.d.L., B.v.H., A.B., M.P.V., and L.G.. J.J.W., T.L., and B.v.H. contributed to the tight-binding simulations without interactions and F.M.C. and A.L.Y. to the minimal model with interactions. J.J.W., F.M.C., A.V., and B.v.H. wrote the manuscript with comments and input from all other co-authors. Nanowires were grown by P.K.. The project was supervised by G.d.L. and B.v.H..

[1] I. Kulik, Macroscopic quantization and the proximity effect in S-N-S junctions, Zh. Eksp. Teor. Fiz. **57**, 1745 (1969) [Sov. J. Exp. Theor. Phys. **30**, 944 (1970)].

[2] C. W. J. Beenakker, Universal limit of critical-current fluctuations in mesoscopic Josephson junctions, Phys. Rev. Lett. **67**, 3836 (1991).

[3] T. M. Klapwijk, Proximity effect from an Andreev perspective, J. Supercond. **17**, 593 (2004).

[4] L. Bretheau, Ç. Ö. Girit, H. Pothier, D. Esteve, and C. Urbina, Exciting Andreev pairs in a superconducting atomic contact, Nature (London) **499**, 312 (2013).

[5] C. Janvier, L. Tosi, L. Bretheau, Ç. Ö. Girit, M. Stern, P. Bertet, P. Joyez, D. Vion, D. Esteve, M. F. Goffman, H. Pothier, and C. Urbina, Coherent manipulation of Andreev states in superconducting atomic contacts, Science **349**, 1199 (2015).

[6] L. Bretheau, Ç. Ö. Girit, C. Urbina, D. Esteve, and H. Pothier, Supercurrent spectroscopy of Andreev states, Phys. Rev. X **3**, 041034 (2013).

[7] D. J. van Woerkom, A. Proutski, B. van Heck, D. Bouman, J. I. Väyrynen, L. I. Glazman, P. Krogstrup, J. Nygård, L. P. Kouwenhoven, and A. Geresdi, Microwave spectroscopy of spinful Andreev bound states in ballistic semiconductor Josephson junctions, Nat. Phys. **13**, 876 (2017).

[8] M. Hays, G. de Lange, K. Serniak, D. J. van Woerkom, D. Bouman, P. Krogstrup, J. Nygård, A. Geresdi, and M. H. Devoret, Direct microwave measurement of

Andreev-bound-state dynamics in a proximitized semiconducting nanowire, Phys. Rev. Lett. **121**, 047001 (2018).

[9] L. Tosi, C. Metzger, M. F. Goffman, C. Urbina, H. Pothier, S. Park, A. L. Yeyati, J. Nygård, and P. Krogstrup, Spin-orbit splitting of Andreev states revealed by microwave spectroscopy, Phys. Rev. X **9**, 011010 (2019).

[10] M. Hays, V. Fatemi, K. Serniak, D. Bouman, S. Diamond, G. de Lange, P. Krogstrup, J. Nygård, A. Geresdi, and M. H. Devoret, Continuous monitoring of a trapped, superconducting spin, Nat. Phys. **16**, 1103 (2020).

[11] M. Hays, V. Fatemi, D. Bouman, J. Cerrillo, S. Diamond, K. Serniak, T. Connolly, P. Krogstrup, J. Nygård, A. Levy Yeyati, A. Geresdi, and M. H. Devoret, Coherent manipulation of an Andreev spin qubit, Science **373**, 430 (2021).

[12] C. Metzger, S. Park, L. Tosi, C. Janvier, A. A. Reynoso, M. F. Goffman, C. Urbina, A. LevyYeyati, and H. Pothier, Circuit-QED with phase-biased Josephson weak links, Phys. Rev. Res. **3**, 013036 (2021).

[13] J. J. Wesdorp, L. Grünhaupt, A. Vaartjes, M. Pita-Vidal, A. Bargerbos, L. J. Splitthoff, P. Krogstrup, B. van Heck, and G. de Lange, Dynamical polarization of the fermion parity in a nanowire Josephson junction, Phys. Rev. Lett. **131**, 117001 (2023).

[14] V. Fatemi, P. D. Kurilovich, M. Hays, D. Bouman, T. Connolly, S. Diamond, N. E. Frattini, V. D. Kurilovich, P. Krogstrup, J. Nygård, A. Geresdi, L. I. Glazman, and M. H. Devoret, Microwave susceptibility observation of interacting many-body Andreev states, Phys. Rev. Lett. **129**, 227701 (2022).

[15] F. J. Matute-Cañadas, C. Metzger, S. Park, L. Tosi, P. Krogstrup, J. Nygård, M. F. Goffman, C. Urbina, H. Pothier, and A. L. Yeyati, Signatures of interactions in the Andreev spectrum of nanowire Josephson junctions, Phys. Rev. Lett. **128**, 197702 (2022).

[16] L. P. Gor'kov and E. I. Rashba, Superconducting 2D system with lifted spin degeneracy: Mixed singlet-triplet state, Phys. Rev. Lett. **87**, 037004 (2001).

[17] C. R. Reeg and D. L. Maslov, Proximity-induced triplet superconductivity in Rashba materials, Phys. Rev. B **92**, 134512 (2015).

[18] R. M. Lutchyn, J. D. Sau, and S. DasSarma, Majorana fermions and a topological phase transition in semiconductor-superconductor heterostructures, Phys. Rev. Lett. **105**, 077001 (2010).

[19] Y. Oreg, G. Refael, and F. von Oppen, Helical liquids and Majorana bound states in quantum wires, Phys. Rev. Lett. **105**, 177002 (2010).

[20] J. Alicea, Majorana fermions in a tunable semiconductor device, Phys. Rev. B **81**, 125318 (2010).

[21] A. C. Potter and P. A. Lee, Majorana end states in multiband microstructures with Rashba spin-orbit coupling, Phys. Rev. B **83**, 094525 (2011).

[22] N. Read and D. Green, Paired states of fermions in two dimensions with breaking of parity and time-reversal symmetries, and the fractional quantum Hall effect, Phys. Rev. B **61**, 10267 (2000).

[23] D. A. Ivanov, Non-Abelian statistics of half-quantum vortices in *p*-wave superconductors, Phys. Rev. Lett. **86**, 268 (2001).

[24] A. Kitaev, Unpaired Majorana fermions in quantum wires, Phys. Usp. **44**, 131 (2001).

[25] I. V. Krive, L. Y. Gorelik, R. I. Shekhter, and M. Jonson, Chiral symmetry breaking and the Josephson current in a ballistic superconductor–quantum wire–superconductor junction, Low Temp. Phys. **30**, 398 (2004).

[26] A. I. Buzdin, Proximity effects in superconductor-ferromagnet heterostructures, Rev. Mod. Phys. **77**, 935 (2005).

[27] A. A. Reynoso, G. Usaj, C. A. Balseiro, D. Feinberg, and M. Avignon, Anomalous Josephson current in junctions with spin polarizing quantum point contacts, Phys. Rev. Lett. **101**, 107001 (2008).

[28] T. Yokoyama, M. Eto, and Y. V. Nazarov, Anomalous Josephson effect induced by spin-orbit interaction and Zeeman effect in semiconductor nanowires, Phys. Rev. B **89**, 195407 (2014).

[29] F. Konschelle, I. V. Tokatly, and F. S. Bergeret, Theory of the spin-galvanic effect and the anomalous phase shift φ_0 in superconductors and Josephson junctions with intrinsic spin-orbit coupling, Phys. Rev. B **92**, 125443 (2015).

[30] T. S. Khaire, M. A. Khasawneh, W. P. Pratt, and N. O. Birge, Observation of spin-triplet superconductivity in Co-based Josephson junctions, Phys. Rev. Lett. **104**, 137002 (2010).

[31] J. W. A. Robinson, J. D. S. Witt, and M. G. Blamire, Controlled injection of spin-triplet supercurrents into a strong ferromagnet, Science **329**, 59 (2010).

[32] D. Sprungmann, K. Westerholt, H. Zabel, M. Weides, and H. Kohlstedt, Evidence for triplet superconductivity in Josephson junctions with barriers of the ferromagnetic Heusler alloy Cu_2MnAl, Phys. Rev. B **82**, 060505(R) (2010).

[33] J. Linder and J. W. A. Robinson, Superconducting spintronics, Nat. Phys. **11**, 307 (2015).

[34] K.-R. Jeon, X. Montiel, S. Komori, C. Ciccarelli, J. Haigh, H. Kurebayashi, L. F. Cohen, A. K. Chan, K. D. Stenning, C.-M. Lee, M. Eschrig, M. G. Blamire, and J. W. A. Robinson, Tunable pure spin supercurrents and the demonstration of their gateability in a spin-wave device, Phys. Rev. X **10**, 031020 (2020).

[35] R. Cai, Y. Yao, P. Lv, Y. Ma, W. Xing, B. Li, Y. Ji, H. Zhou, C. Shen, S. Jia, X. C. Xie, I. Žutić, Q.-F. Sun, and W. Han, Evidence for anisotropic spin-triplet Andreev reflection at the 2D van der Waals ferromagnet/superconductor interface, Nat. Commun. **12**, 6725 (2021).

[36] G. Yang, C. Ciccarelli, and J. W. A. Robinson, Boosting spintronics with superconductivity, APL Mater. **9**, 050703 (2021).

[37] H. G. Ahmad, M. Minutillo, R. Capecelatro, A. Pal, R. Caruso, G. Passarelli, M. G. Blamire, F. Tafuri, P. Lucignano, and D. Massarotti, Coexistence and tuning of spin-singlet and triplet transport in spin-filter Josephson junctions, Commun. Phys. **5**, 2 (2022).

[38] D. B. Szombati, S. Nadj-Perge, D. Car, S. R. Plissard, E. P. A. M. Bakkers, and L. P. Kouwenhoven, Josephson Φ_0-junction in nanowire quantum dots, Nat. Phys. **12**, 568 (2016).

[39] E. Strambini, A. Iorio, O. Durante, R. Citro, C. Sanz-Fernández, C. Guarcello, I. V. Tokatly, A. Braggio, M. Rocci, N. Ligato, V. Zannier, L. Sorba, F. S. Bergeret, and F. Giazotto, A Josephson phase battery, Nat. Nanotechnol. **15**, 656 (2020).

[40] W. Mayer, M. C. Dartiailh, J. Yuan, K. S. Wickramasinghe, E. Rossi, and J. Shabani, Gate controlled anomalous phase

shift in Al/InAs Josephson junctions, Nat. Commun. **11**, 212 (2020).

[41] D. Phan, J. Senior, A. Ghazaryan, M. Hatefipour, W. M. Strickland, J. Shabani, M. Serbyn, and A. P. Higginbotham, Detecting induced $p \pm ip$ pairing at the Al-InAs interface with a quantum microwave circuit, Phys. Rev. Lett. **128**, 107701 (2022).

[42] G. Wang, T. Dvir, G. P. Mazur, C.-X. Liu, and N. van Loo, Singlet and triplet Cooper pair splitting in superconducting-semiconducting hybrid nanowires, Nature **612**, 448 (2022).

[43] L. I. Glazman and G. Catelani, Bogoliubov quasiparticles in superconducting qubits, SciPost Phys. Lect. Notes, 31 (2021).

[44] M. Pita-Vidal, A. Bargerbos, C.-K. Yang, D. J. van Woerkom, W. Pfaff, N. Haider, P. Krogstrup, L. P. Kouwenhoven, G. de Lange, and A. Kou, A gate-tunable, field-compatible fluxonium, Phys. Rev. Appl. **14**, 064038 (2020).

[45] See Supplemental Material at http://link.aps.org/supplemental/10.1103/PhysRevB.109.045302, which additionally includes Refs. [93–103].

[46] A. J. Annunziata, D. F. Santavicca, L. Frunzio, G. Catelani, M. J. Rooks, A. Frydman, and D. E. Prober, Tunable superconducting nanoinductors, Nanotechnology **21**, 445202 (2010).

[47] J. G. Kroll, F. Borsoi, K. L. van der Enden, W. Uilhoorn, D. de Jong, M. Quintero-Pérez, D. J. van Woerkom, A. Bruno, S. R. Plissard, D. Car, E. P. A. M. Bakkers, M. C. Cassidy, and L. P. Kouwenhoven, Magnetic field resilient superconducting coplanar waveguide resonators for hybrid cQED experiments, Phys. Rev. Appl. **11**, 064053 (2019).

[48] We found that holes closer spaced to the edges of structures reduced the flux jumps significantly, compared to a 1-μm spacing used in Ref. [47].

[49] W. Chang, S. M. Albrecht, T. S. Jespersen, F. Kuemmeth, P. Krogstrup, J. Nygård, and C. M. Marcus, Hard gap in epitaxial semiconductor-superconductor nanowires, Nat. Nanotechnol. **10**, 232 (2015).

[50] A. Benfenati, A. Maiani, F. N. Rybakov, and E. Babaev, Vortex nucleation barrier in superconductors beyond the Bean-Livingston approximation: A numerical approach for the Sphaleron problem in a gauge theory, Phys. Rev. B **101**, 220505(R) (2020).

[51] M. Tinkham, *Introduction to Superconductivity*, 2nd ed., Dover Books on Physics (Dover, Mineola, 2015).

[52] A. Zazunov, V. S. Shumeiko, E. N. Bratus', J. Lantz, and G. Wendin, Andreev level qubit, Phys. Rev. Lett. **90**, 087003 (2003).

[53] L. Bretheau, Localized excitations in superconducting atomic contacts: Probing the andreev doublet, Ph.D. thesis, Ecole Polytechnique, France, 2013.

[54] S. Park, C. Metzger, L. Tosi, M. F. Goffman, C. Urbina, H. Pothier, and A. L. Yeyati, From adiabatic to dispersive readout of quantum circuits, Phys. Rev. Lett. **125**, 077701 (2020).

[55] Y.-J. Doh, Tunable supercurrent through semiconductor nanowires, Science **309**, 272 (2005).

[56] M. F. Goffman, C. Urbina, H. Pothier, J. Nygård, C. M. Marcus, and P. Krogstrup, Conduction channels of an InAs-Al nanowire Josephson weak link, New J. Phys. **19**, 092002 (2017).

[57] Note that the labels can refer either to manifolds that originate from the same transverse subband, due to finite-length effects, or to orbitals from different transverse subbands.

[58] S. Park and A. L. Yeyati, Andreev spin qubits in multichannel Rashba nanowires, Phys. Rev. B **96**, 125416 (2017).

[59] M. Governale and U. Zülicke, Spin accumulation in quantum wires with strong Rashba spin-orbit coupling, Phys. Rev. B **66**, 073311 (2002).

[60] N. M. Chtchelkatchev and Y. V. Nazarov, Andreev quantum dots for spin manipulation, Phys. Rev. Lett. **90**, 226806 (2003).

[61] B. Béri, J. H. Bardarson, and C. W. J. Beenakker, Splitting of Andreev levels in a Josephson junction by spin-orbit coupling, Phys. Rev. B **77**, 045311 (2008).

[62] T. Yokoyama, M. Eto, and Y. V. Nazarov, Josephson Current through semiconductor nanowire with spin-orbit interaction in magnetic field, J. Phys. Soc. Jpn. **82**, 054703 (2013).

[63] F. Konschelle, F. S. Bergeret, and I. V. Tokatly, Semiclassical quantization of spinning quasiparticles in ballistic Josephson junctions, Phys. Rev. Lett. **116**, 237002 (2016).

[64] I. L. Kurland, I. L. Aleiner, and B. L. Altshuler, Mesoscopic magnetization fluctuations for metallic grains close to the Stoner instability, Phys. Rev. B **62**, 14886 (2000).

[65] J. D. S. Bommer, H. Zhang, Ö. Gül, B. Nijholt, M. Wimmer, F. N. Rybakov, J. Garaud, D. Rodic, E. Babaev, M. Troyer, D. Car, S. R. Plissard, E. P. A. M. Bakkers, K. Watanabe, T. Taniguchi, and L. P. Kouwenhoven, Spin-orbit protection of induced superconductivity in Majorana nanowires, Phys. Rev. Lett. **122**, 187702 (2019).

[66] M. W. A. de Moor, J. D. S. Bommer, D. Xu, G. W. Winkler, A. E. Antipov, A. Bargerbos, G. Wang, N. van Loo, R. L. M. Op het Veld, S. Gazibegovic, D. Car, J. A. Logan, M. Pendharkar, J. S. Lee, E. P. A. M Bakkers, C. J. Palmstrøm, R. M. Lutchyn, L. P. Kouwenhoven, and H. Zhang, Electric field tunable superconductor-semiconductor coupling in Majorana nanowires, New J. Phys. **20**, 103049 (2018).

[67] A. Bargerbos, M. Pita-Vidal, R. Žitko, J. Ávila, L. J. Splitthoff, L. Grünhaupt, J. J. Wesdorp, C. K. Andersen, Y. Liu, L. P. Kouwenhoven, R. Aguado, A. Kou, and B. van Heck, Singlet-doublet transitions of a quantum dot Josephson junction detected in a transmon circuit, PRX Quantum **3**, 030311 (2022).

[68] D. Liang and X. P. Gao, Strong tuning of Rashba spin–orbit interaction in single InAs nanowires, Nano Lett. **12**, 3263 (2012).

[69] S. M. Albrecht, A. P. Higginbotham, M. Madsen, F. Kuemmeth, T. S. Jespersen, J. Nygård, P. Krogstrup, and C. M. Marcus, Exponential protection of zero modes in Majorana islands, Nature (London) **531**, 206 (2016).

[70] K. Zuo, V. Mourik, D. B. Szombati, B. Nijholt, D. J. van Woerkom, A. Geresdi, J. Chen, V. P. Ostroukh, A. R. Akhmerov, S. R. Plissard, D. Car, E. P. A. M. Bakkers, D. I. Pikulin, L. P. Kouwenhoven, and S. M. Frolov, Supercurrent interference in few-mode nanowire Josephson junctions, Phys. Rev. Lett. **119**, 187704 (2017).

[71] A. Kringhøj, T. W. Larsen, O. Erlandsson, W. Uilhoorn, J. Kroll, M. Hesselberg, R. McNeil, P. Krogstrup, L. Casparis, C. Marcus, and K. Petersson, Magnetic-field-compatible

superconducting transmon qubit, Phys. Rev. Appl. **15**, 054001 (2021).

[72] W. Uilhoorn, J. G. Kroll, A. Bargerbos, S. D. Nabi, C.-K. Yang, P. Krogstrup, L. P. Kouwenhoven, A. Kou, and G. de Lange, Quasiparticle trapping by orbital effect in a hybrid superconducting-semiconducting circuit, arXiv:2105.11038 [cond-mat].

[73] J. I. Väyrynen, G. Rastelli, W. Belzig, and L. I. Glazman, Microwave signatures of Majorana states in a topological Josephson junction, Phys. Rev. B **92**, 134508 (2015).

[74] L. Fu and C. L. Kane, Josephson current and noise at a superconductor/quantum-spin-Hall-insulator/superconductor junction, Phys. Rev. B **79**, 161408(R) (2009).

[75] B. van Heck, J. I. Väyrynen, and L. I. Glazman, Zeeman and spin-orbit effects in the Andreev spectra of nanowire junctions, Phys. Rev. B **96**, 075404 (2017).

[76] C. Padurariu and Y. V. Nazarov, Theoretical proposal for superconducting spin qubits, Phys. Rev. B **81**, 144519 (2010).

[77] A. Zazunov, R. Egger, T. Jonckheere, and T. Martin, Anomalous Josephson current through a spin-orbit coupled quantum dot, Phys. Rev. Lett. **103**, 147004 (2009).

[78] A. Brunetti, A. Zazunov, A. Kundu, and R. Egger, Anomalous Josephson current, incipient time-reversal symmetry breaking, and Majorana bound states in interacting multilevel dots, Phys. Rev. B **88**, 144515 (2013).

[79] A. A. Reynoso, G. Usaj, C. A. Balseiro, D. Feinberg, and M. Avignon, Spin-orbit-induced chirality of Andreev states in Josephson junctions, Phys. Rev. B **86**, 214519 (2012).

[80] F. S. Bergeret and I. V. Tokatly, Theory of diffusive ϕ_0 Josephson junctions in the presence of spin-orbit coupling, Europhys. Lett. **110**, 57005 (2015).

[81] G. Campagnano, P. Lucignano, D. Giuliano, and A. Tagliacozzo, Spin–orbit coupling and anomalous Josephson effect in nanowires, J. Phys.: Condens. Matter **27**, 205301 (2015).

[82] J.-F. Liu and K. S. Chan, Relation between symmetry breaking and the anomalous Josephson effect, Phys. Rev. B **82**, 125305 (2010).

[83] A. Rasmussen, J. Danon, H. Suominen, F. Nichele, M. Kjaergaard, and K. Flensberg, Effects of spin-orbit coupling and spatial symmetries on the Josephson current in SNS junctions, Phys. Rev. B **93**, 155406 (2016).

[84] A. Assouline, C. Feuillet-Palma, N. Bergeal, T. Zhang, A. Mottaghizadeh, A. Zimmers, E. Lhuillier, M. Eddrie, P. Atkinson, M. Aprili, and H. Aubin, Spin-orbit induced phase-shift in Bi_2Se_3 Josephson junctions, Nat. Commun. **10**, 126 (2019).

[85] T. Ö. Rosdahl, A. Vuik, M. Kjaergaard, and A. R. Akhmerov, Andreev rectifier: A nonlocal conductance signature of topological phase transitions, Phys. Rev. B **97**, 045421 (2018).

[86] L. J. Splitthoff, A. Bargerbos, L. Grünhaupt, M. Pita-Vidal, J. J. Wesdorp, Y. Liu, A. Kou, C. K. Andersen, and B. van Heck, Gate-tunable kinetic inductance in proximitized nanowires, Phys. Rev. Appl. **18**, 024074 (2022).

[87] Y. Peng, F. Pientka, E. Berg, Y. Oreg, and F. von Oppen, Signatures of topological Josephson junctions, Phys. Rev. B **94**, 085409 (2016).

[88] C. Murthy, V. D. Kurilovich, P. D. Kurilovich, B. van Heck, L. I. Glazman, and C. Nayak, Energy spectrum and current-phase relation of a nanowire Josephson junction close to the topological transition, Phys. Rev. B **101**, 224501 (2020).

[89] G. W. Winkler, A. E. Antipov, B. van Heck, A. A. Soluyanov, L. I. Glazman, M. Wimmer, and R. M. Lutchyn, A unified numerical approach to semiconductor-superconductor heterostructures, Phys. Rev. B **99**, 245408 (2019).

[90] D. Laroche, D. Bouman, D. J. van Woerkom, A. Proutski, C. Murthy, D. I. Pikulin, C. Nayak, R. J. J. van Gulik, J. Nygård, P. Krogstrup, L. P. Kouwenhoven, and A. Geresdi, Observation of the 4π-periodic Josephson effect in indium arsenide nanowires, Nat. Commun. **10**, 245 (2019).

[91] G. Burkard, T. D. Ladd, J. M. Nichol, A. Pan, and J. R. Petta, Semiconductor spin qubits, Rev. Mod. Phys. **95**, 025003 (2023).

[92] C. Padurariu and Y. V. Nazarov, Spin blockade qubit in a superconducting junction, Europhys. Lett. **100**, 57006 (2012).

[93] J. H. Plantenberg, Coupled superconducting flux qubits, Ph.D. thesis, Delft University of Technology, 2007.

[94] *The SQUID Handbook: Fundamentals and Technology of SQUIDs and SQUID Systems*, edited by J. Clarke and A. I. Braginski, 1st ed. (Wiley, New York, 2004).

[95] N. Samkharadze, A. Bruno, P. Scarlino, G. Zheng, D. P. DiVincenzo, L. DiCarlo, and L. M. K. Vandersypen, High-kinetic-inductance superconducting nanowire resonators for circuit QED in a magnetic field, Phys. Rev. Appl. **5**, 044004 (2016).

[96] J. J. Wesdorp and G. de Lange, Superconducting quantum interference devices and uses thereof (2020), Patent pending: WO2022058025A1, EP4214644A1, AU2020467946A1, KR20230069112A.

[97] A. E. Antipov, A. Bargerbos, G. W. Winkler, B. Bauer, E. Rossi, and R. M. Lutchyn, Effects of gate-induced electric fields on semiconductor Majorana nanowires, Phys. Rev. X **8**, 031041 (2018).

[98] M. S. Khalil, M. J. A. Stoutimore, F. C. Wellstood, and K. D. Osborn, An analysis method for asymmetric resonator transmission applied to superconducting devices, J. Appl. Phys. **111**, 054510 (2012).

[99] C. W. Groth, M. Wimmer, A. R. Akhmerov, and X. Waintal, KWANT: A software package for quantum transport, New J. Phys. **16**, 063065 (2014).

[100] T. Laeven, B. Nijholt, M. Wimmer, and A. R. Akhmerov, Enhanced proximity effect in zigzag-shaped Majorana Josephson junctions, Phys. Rev. Lett. **125**, 086802 (2020).

[101] C. W. J. Beenakker and H. van Houten, *Single-Electron Tunneling and Mesoscopic Devices*, edited by H. Koch and H. Lubbig (Springer, Berlin, 1992).

[102] G. Katsaros, J. Kukučka, L. Vukušić, H. Watzinger, F. Gao, T. Wang, J.-J. Zhang, and K. Held, Zero field splitting of heavy-hole states in quantum dots, Nano Lett. **20**, 5201 (2020).

[103] M. Newville, R. Otten, A. Nelson, A. Ingargiola, T. Stensitzki, D. Allan, A. Fox, F. Carter, Michał, R. Osborn, D. Pustakhod, Lneuhaus, S. Weigand, Glenn, C. Deil, Mark, A. L. R. Hansen, G. Pasquevich, L. Foks, N. Zobrist *et al.*, Lmfit/lmfit-py: 1.0.3, Zenodo (2021).

[104] https://www.doi.org/10.4121/20311137.